Journal of Luminescence 256 (2023) 119651

Contents lists available at ScienceDirect

Journal of Luminescence

journal homepage: www.elsevier.com/locate/jlumin

Full Length Article

Photoluminescence properties of InP/GaP/ZnS core/shell/shell colloidal quantum dots treated with halogen acids

Yanqing Zhu [a], Cong Shen [a,b,1], Xueqing Xu [a,*], Jianhua Zou [c], Lei Wang [c], Xudong Cheng [a], Jingqiu Liang [d], Xiudi Xiao [a], Gang Xu [a,**]

[a] Guangzhou Institute of Energy Conversion, Key Laboratory of Renewable Energy, Guangdong Provincial Key Laboratory of New and Renewable Energy Research and Development, Chinese Academy of Sciences, Guangzhou, 510640, PR China
[b] University of Chinese Academy of Sciences, Beijing, 100049, PR China
[c] Guangzhou New Vision Opto-Electronic Technology Co., Ltd., Guangzhou, 510530, PR China
[d] Changchun Institute of Optics, Fine Mechanics and Physics, Chinese Academy of Sciences, Changchun, 130033, PR China

ARTICLE INFO

Keywords:
InP
Quantum dots
Halogen acids
Photoluminescence
Recombination

ABSTRACT

InP quantum dots (QDs) with low toxicity are considered to be the most promising materials. However, the oxidation problem of In and P has become to the major factor affecting the optical properties of InP QDs. In this work, the effect of luminescence properties of InP/GaP/ZnS QDs with halogen acid treatment have been studied. The results show that HF and HCl are beneficial to improve the optical properties of QDs, HBr especially HI are not conductive to promote the photoluminescence quantum yield (PL QY) of QDs. HF and HCl can etch the oxidative layer effectively, the F^- and Cl^- can also passivate the surface indium dangling bonds in the form of atomic ligands. The proposed model of charge carrier recombination show that the PL QY improved significantly after HA treatment attributed to the recombination of electron-hole pairs through radiative pathways mainly from the conduction band and valence band. The InP QDs with HF treatment has the best luminescence properties with high PL QY of 96%, offering great potential for advanced optoelectronic devices.

1. Introduction

Quantum dots (QDs) which have the characteristics of adjustable luminescence wavelength, high photoluminescence, wide color gamut and solution processability are highly competitive candidates for new display materials [1–3]. At present, Cadmium QDs and perovskite QDs with excellent optical property are limited in practical application because of their toxic elements (cadmium and lead) [4–8]. Therefore, environmentally friendly QDs materials mainly including group II-VI (such as ZnSe and ZnS) [9–11] and III-V (such as InP and InAs) [12–14] materials have been studied. Compared with II-VI QDs, III-V QDs have many incomparable advantages such as large Bohr radius and stronger quantum effect. InP QDs which have the characteristics of low toxicity and emission spectrum tunability ranging from visible to near-infrared region are considered to be the most promising materials [15–17].

During the synthesis of InP QDs, In and P are easy to oxidize to form oxidation defects such as PO_4, In_2O_3 or InP_xO_y [18–20], which are suspected to the major reason of the poor optical properties of InP QDs. Therefore, the oxidation defects must be removed to improve the optical properties of InP QDs. To improve the optical properties of InP QDs, scientists have taken many methods such as shell coating, cation doping, surface passivation, acid treatment [21–26]. Among them, acid treatment is a predominant strategy to etch oxidation. Many researchers have made a series of progress in treating InP QDs with HF. In 1996, Micic et al. introduced HF to remove the defect states on the surface, and a photoluminescence quantum yield (PL QY) of InP QDs of 30% had been obtained at a room temperature [27]. Kim et al. demonstrated that very significant luminescence enhancements occur at lower HF exposure, due to the fluoride ions passivated the surface indium dangling bonds in the form of atomic ligands [28]. Jang et al. added HF to etch out the oxidative InP core surface during the growth of the initial ZnSe shell, and finally prepared a uniform InP core and a highly symmetrical core/shell QDs with a quantum yield of approximately 100% [13]. In

* Corresponding author.
** Corresponding author.
E-mail addresses: xuxq@ms.giec.ac.cn (X. Xu), xugang@ms.giec.ac.cn (G. Xu).
[1] Yanqing Zhu and Cong Shen have contributed equally to this work.

https://doi.org/10.1016/j.jlumin.2022.119651
Received 27 June 2022; Received in revised form 15 December 2022; Accepted 26 December 2022
Available online 26 December 2022

addition to HF, the treatment of InP nanowires with HBr and HCl has been studied. Berg et al. researched the influence of HBr in situ etching on the growth of InP nanowires, and pointed that using of HBr can removed the defect-related luminescence due to parasitic radial growth [29]. Thuy et al. reported InP nanowires in situ etching with HCl at a high growth temperature, and the impurity-contaminated sidewall can be etched away [30]. In addition to the above halogen acids, researchers rarely use HI to treat InP QDs, but the role of iodide in InP QDs synthesis has been studied. Sun et al. chose ZnI_2 and InI_3 as precursors to obtain InP/ZnS QDs with a shorter emission wavelength, and pointed that iodide with weak binding energy could result a fast reaction rate and small particle size QDs [25]. In summary, HF can effectively remove the oxidative layer of InP QDs, HBr and HCl can be used to treat InP nanowires, HI has not been studied in the treatment of InP. In other words, halogen acids can be used to treat InP QDs, but the effect of halogen acids has not been systematically studied.

In this work, we have systematically studied the effect of luminescence properties of InP/GaP/ZnS QDs with halogen acid treatment. The InP/GaP/ZnS QDs with HF, HCl, HBr and HI have been synthesized respectively by halogen acid in-situ injection method, which can prevent the reoxidation of InP core due to exposure to air. The effects of different halogen acid on the treatment of InP QDs have been analyzed by UV, PL, TEM, XRD, XPS measurement. The results show the HF and HCl are beneficial to improve the optical properties of QDs, HBr especially HI are not conductive to promote the PL QY of QDs. HF and HCl can etch the oxidative layer effectively, the F^- and Cl^- can also passivate the surface indium dangling bonds in the form of atomic ligands. The effect of HA treatment on the electron-hole pairs recombination dynamics of InP-HA/GaP/ZnS has been investigated using transient PL spectra and a model of various charge carrier recombination process has been proposed. After HA treatment, the PL QY improved significantly which can be attributed to the recombination of electron-hole pairs through radiative pathways mainly from the CB and VB. The InP QDs with HF treatment has the best luminescence properties with high PL QY of 96%, offering great potential for advanced optoelectronic devices.

2. Experimental section

2.1. Materials

Indium acetate ($In(Ac)_3$, 99.99% metals basis) was purchased from Sigma Aldrich. Tris (trimethylsily)phosphine ($(TMS)_3P$, 10 wt % in hexane, 98%) was purchased from Stream Chemicals. Zinc acetate ($Zn(Ac)_2$, 99.99% metals basis), lauric acid (LA, ≥99%), 1-octadecene (ODE, ≥90%), 1-octanethiol (OT, ≥98%), Gallium chloride ($GaCl_3$,99.999% metals basis), hydrofluoric acid (HF, 40 wt%), hydrochloric acid (HCl, 36.0–38.0 wt%), hydrobromic acid (HBr, 48 wt%), hydroiodic acid (HI, 55.0–58.0 wt%) were purchased from Aladdin Chemistry Co., Ltd. N-hexane, anhydrous alcohol and acetone were purchased from Guangzhou Chemical Reagent Co., Ltd. All chemical reagents were used without further processing and purification.

2.2. Preparation of precursors

Stock solution for P precursor: 1.3 mmol $(TMS)_3P$ was mixed with 5 mL of ODE in a 12 mL glass bottle in a nitrogen-filled glove box.

Stock solution of Ga precursor: 0.68 mmol $GaCl_3$ were added in 8 mL ODE from a nitrogen-filled glove box, and the solution was treated with ultrasonication under 40 °C heating.

Stock solution of LA: 2.16 mmol LA were added in 8 mL ODE, and the solution was treated with ultrasonication.

Stock solution of halogen acid (HA): 0.50 mL (11.20 mmol) hydrofluoric acid, 0.95 mL (11.20 mmol) hydrochloric acid, 1.27 mL (11.20 mmol) hydrobromic acid, and 0.50 mL (11.20 mmol) hydroiodic acid were added in 5 mL acetone respectively to form the corresponding halogen acid solutions.

2.3. Synthesis of InP core

$In(Ac)_3$ (17.52 mg, 0.06 mmol), $Zn(Ac)_2$ (45.87 mg, 0.25 mmol), and LA (108.67 mg, 0.54 mmol) were mixed to 4 mL of ODE in a 25 mL three-neck flask. The mixture was degassed under vacuum at 120 °C for 30 min and purged with nitrogen, repeated this process three times. The resulting solution was added 0.5 mL P precursor, and then the mixture was heated to 250 °C. The solution was maintained at 250 °C for 5 min, and an aliquot was taken from the sample.

2.4. Synthesis of InP/GaP/ZnS QDs

0.2 mL Ga precursor was added in the above InP core solution at 250 °C for 10 min. Then 0.3 mmol OT was quickly injected to the mixture and maintained for 10 min at 250 °C. At the end of the reaction, the resulting solution was cooled down. The obtained InP/GaP/ZnS QDs were dissolved in n-hexane and precipitated by the addition of excess acetone, and centrifuged at 8000 rpm for 5 min, the supernatant was decanted, and then the precipitate was re-dispersed in n-hexane. The purification process was repeated three times. The purified InP/GaP/ZnS QDs dissolved in n-hexane for further characterization.

2.5. Synthesis of InP/GaP/ZnS QDs with halogen acid treatment

After the mixture was heated to 250 °C in the above InP core process, 0.8 mL LA stock solution was added in the mixture. After 5 min at 250 °C, 0.2 mL hydrofluoric acid stock solution was injected in the mixture and was mixed for 5 min to obtain InP–HF core. Then 0.3 mmol OT was quickly injected to the mixture and maintained for 10 min at 250 °C. Finally, the resulting solution was cooled down to end the reaction. InP/GaP/ZnS QDs with hydrofluoric acid treatment (called InP–HF/GaP/ZnS QDs) were obtained after the purification process.

Using hydrochloric acid, hydrobromic acid, and hydroiodic acid stock solution instead of hydrofluoric acid stock solution, the InP core etched with halogen acid called InP-HA core (referred to InP–HF core, InP–HCl core, InP–HBr core, InP–HI core). InP/GaP/ZnS QDs with corresponding halogen acid treatment called InP-HA/GaP/ZnS QDs (referred to InP–HCl/GaP/ZnS QDs, InP–HBr/GaP/ZnS QDs, InP–HI/GaP/ZnS QDs) were obtained respectively.

2.6. Characterization

Optical absorption spectra were recorded on a PerkinElmer Lambda 750 spectrophotometer. The PL spectra and absolute PL QY of QDs dispersed in hexane were recorded at 365 nm excitation using the FLS980 fluorescence spectrometer equipped with an integrating sphere from Edinburgh Instruments Ltd. Transient PL spectra were measured at room temperature using the FLS980 fluorescence spectrometer equipped with a time-correlated single-photon counting (TCSPC) spectrofluorometer from Edinburgh Instruments Ltd, and the QDs were excited by a 405 nm ps laser diode with a 2 MHz repetition rate. X-ray diffraction (XRD) measurements were performed on a Smartlab X-ray diffractometer from Rigaku Corporation operated at 40 KeV and 40 mA with Cu Kα radiation ($\lambda = 1.5406$ Å). High-resolution transmission electron microscope (HRTEM) images were taken on a JEM-2100F TEM from JEOL. The size distributions of QDs were estimated with the software of Nanomeasure.

3. Results and discussion

The schematic of synthesis process of InP-HA/GaP/ZnS QDs is shown in Scheme 1. InP core was synthesized by a heating up method using Indium acetate and $(TMS)_3P$ as precursors, and lauric acid as surface ligand. InP-HA core was obtained by injecting the halogen acid directly, which can avert the risk of oxidation of InP core due to exposure to air. In order to avoid precipitation of QDs and ensure that there are enough

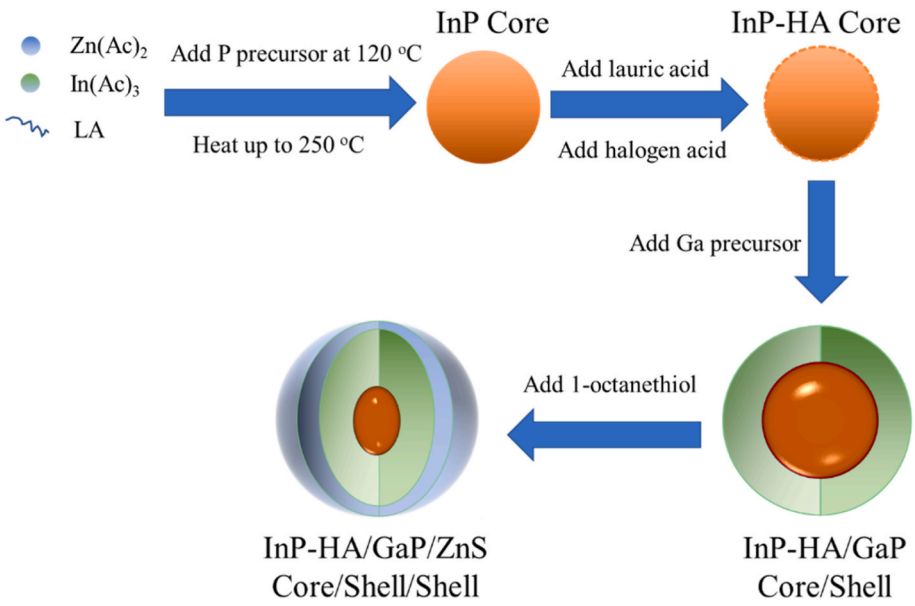

Scheme 1. The synthesis process of InP-HA/GaP/ZnS QDs.

ligands in the reaction system, the lauric acid was added before halogen acid treatment. Then Gallium chloride was added to from a GaP shell to reduce the lattice mismatch between InP-HA core and ZnS shell. Finally, the ZnS shell was obtained by added 1-octanethiol quickly, and the InP-HA/GaP/ZnS QDs were obtained.

In order to investigate the spectral properties of InP-HA/GaP/ZnS QDs, InP core, InP-HA core, InP-HA/GaP, InP-HA/GaP/ZnS were sampled and detected in the synthesis process. The absorption and PL spectra of the InP, InP/GaP, InP/GaP/ZnS without and with halogen acid etched are depicted in Figs. 1 and 2. It should be noted that absorption and PL peaks of InP–HI core and InP–HI/GaP cannot be measured after purification, so the corresponding samples without

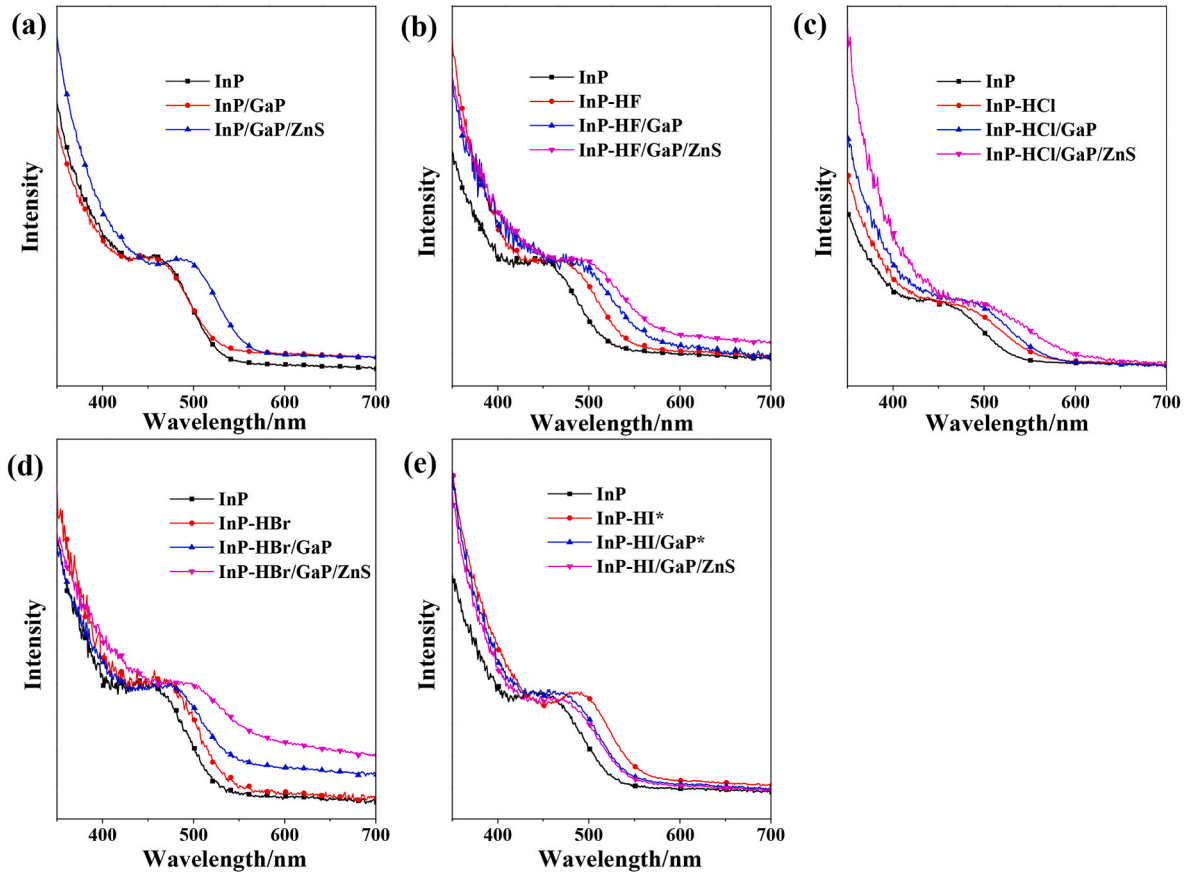

Fig. 1. (a)The absorption spectra of InP, InP/GaP and InP/GaP/ZnS. The absorption spectra of InP, InP-HA, InP-HA/GaP, InP-HA/GaP/ZnS with (b) HF, (c) HCl, (d) HBr, and (e) HI etched. (* represents the unpurified sample).

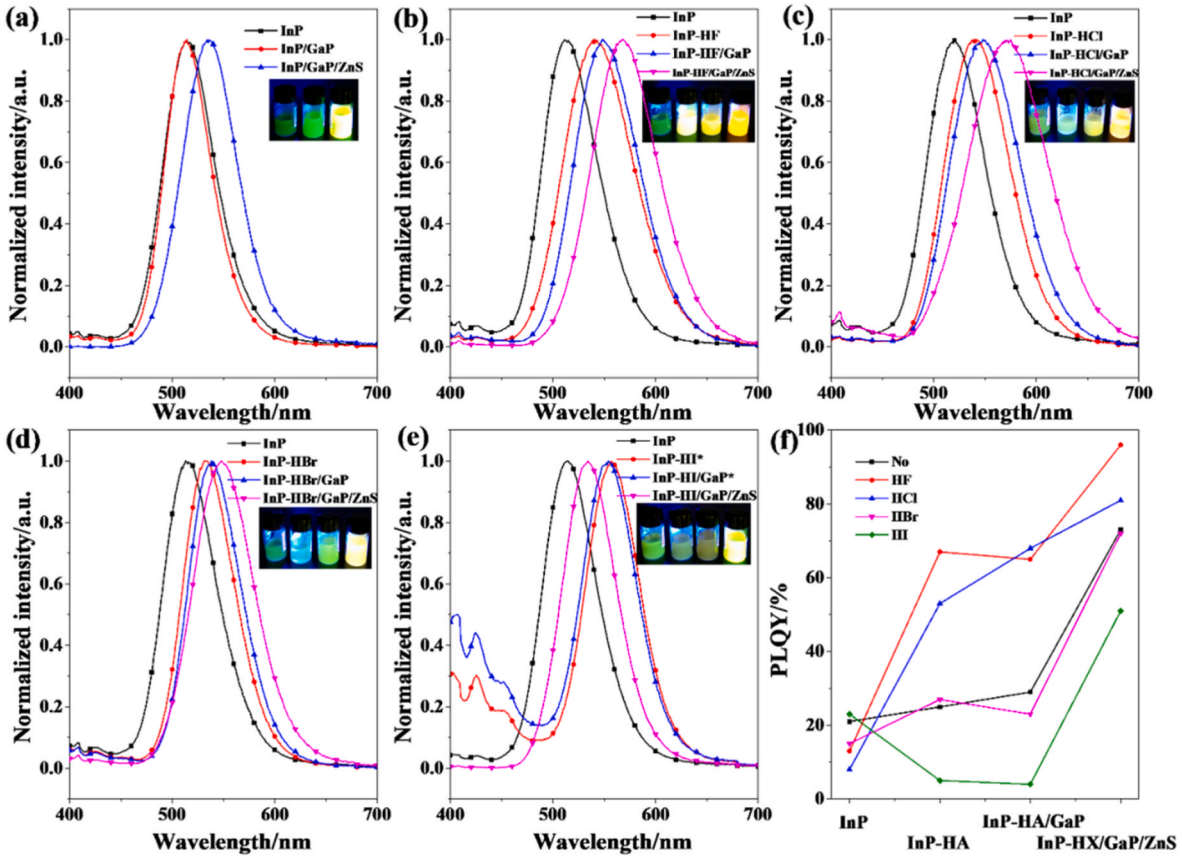

Fig. 2. (a) The PL spectra of InP, InP/GaP and InP/GaP/ZnS (inset: Photograph of InP, InP/GaP and InP/GaP/ZnS taken under 365 nm illumination). The PL spectra of InP, InP-HA, InP-HA/GaP, InP-HA/GaP/ZnS with (b) HF, (c) HCl, (d) HBr, and (e) HI etched (inset: Photographs of InP, InP-HA, InP-HA/GaP and InP-HA/GaP/ZnS taken under 365 nm illumination. * represents the unpurified sample). (f) PLQY of InP/GaP/ZnS and InP-HA/GaP/ZnS with different halogen acid.

purification have been measured, while all the other samples have been purified. Figs. 1(a) and Figure 2(a) show the absorption of the QDs without halogen acid etched, typical shoulder peaks can be observed together with absorption tails extended to longer wavelength. The absorption and PL peaks were almost the same location at about 457 nm and 514 nm after coating the GaP shell, and shifted red to 484 nm and 536 nm after coating the ZnS shell. From Fig. 1(b–d) and Fig. 2(b–d), the absorption peaks of QDs with halogen acid etched all shifted red along with HF, HCl and HBr treatment and shells coating. For InP/GaP/ZnS treated with HF, a shape absorption and PL peaks of InP core located at about 448 nm and 512 nm, the peaks shifted to about 465 nm and 540 nm after HF treated correspondingly. The red shift indicate that the InP core continue to grow while HF etching, which can be confirmed by TEM images. The sizes of InP–HF cores are larger than that of InP cores as shown in Fig. S1. After coating with GaP and ZnS shells, the absorption and PL peaks shifted to about 494 nm and 567 nm, which is associated with the delocalization of the carrier wave functions from the core only region to the outer shell region [31]. For InP/GaP/ZnS treated with HCl and HBr, the absorption and PL peaks have the same trend as InP/GaP/ZnS treated with HF. From Figs. 1(e) and 2(e), the samples of InP–HI and InP–HI/GaP without purification have been tested, because the absorption and PL spectra could not be tested after purification. The shape absorption and PL peaks of InP core located at about 442 nm and 512 nm, the peaks shifted to about 486 nm and 557 nm after HI treated correspondingly. The absorption peak is enhanced, but the emission peak is weakened, that is because lot of defects existed in the InP–HI core, which can be confirmed from the transient PL spectra showed in Fig. 6(e). Different from the red shift of InP/GaP/ZnS QDs with HF, HCl and HBr treatment, the absorption and PL peaks of InP–HI/GaP/ZnS shifted blue to about 462 nm and 534 nm after coating with GaP and ZnS shells, which was related to the lack of purification of InP–HI and InP–HI/GaP.

The PL spectra and PL QY of the InP, InP/GaP, InP/GaP/ZnS without and with halogen acid etched are depicted in Fig. 2. The full width half maximum (FWHM) value of InP/GaP/ZnS was about 63 nm. However, the FWHM values of InP-HA/GaP/ZnS became 76 nm, 91 nm, 70 nm and 64 nm after HF, HCl, HBr, HI treatment. That is to say, the FWHM value became wider after halogen acid treatment. Take QDs treated with HF for example, the FWHM values of InP core, InP–HF, InP–HF/GaP and InP–HF/GaP/ZnS were 64 nm, 80 nm, 76 nm and 76 nm, respectively. That was because the size distribution of InP core became broader, which could be reflected by TEM results. From Fig. S1, the size distribution of InP core became uneven after HF etching, therefore the size distribution of QDs is relatively wide after shell coating, which caused a large FWHM value. The size uniformity of QDs can be improved by accurately controlling temperature, stirring speed and halogen acid injection speed.

In order to survey the size distribution of QDs, TEM tests of InP/GaP/ZnS QDs before and after HA treatment have been carried out, as shown in Fig. 3. The average size InP/GaP/ZnS QDs is 4.8 ± 1.59 nm with the relative standard deviation of 33%. After treated with HF, HCl, HBr, HI, the average size distributions of InP-HA/GaP/ZnS QDs became 3.75 ± 1.30 nm, 4.88 ± 1.67 nm, 4.19 ± 1.57 nm, 3.56 ± 1.27 nm with the relative standard deviation of 34%, 34%, 37%, 35%, respectively. The uniformity of quantum dots after HA treatment is slightly worse than that without etching. Inset images at the top right of TEM images in Fig. 3 are the correspond high-resolution transmission electron microscopy (HR-TEM) images, which showed that InP/GaP/ZnS QDs before and after HA treatment all possessed great crystallinity due to the obvious lattice fringe on the QDs surface.

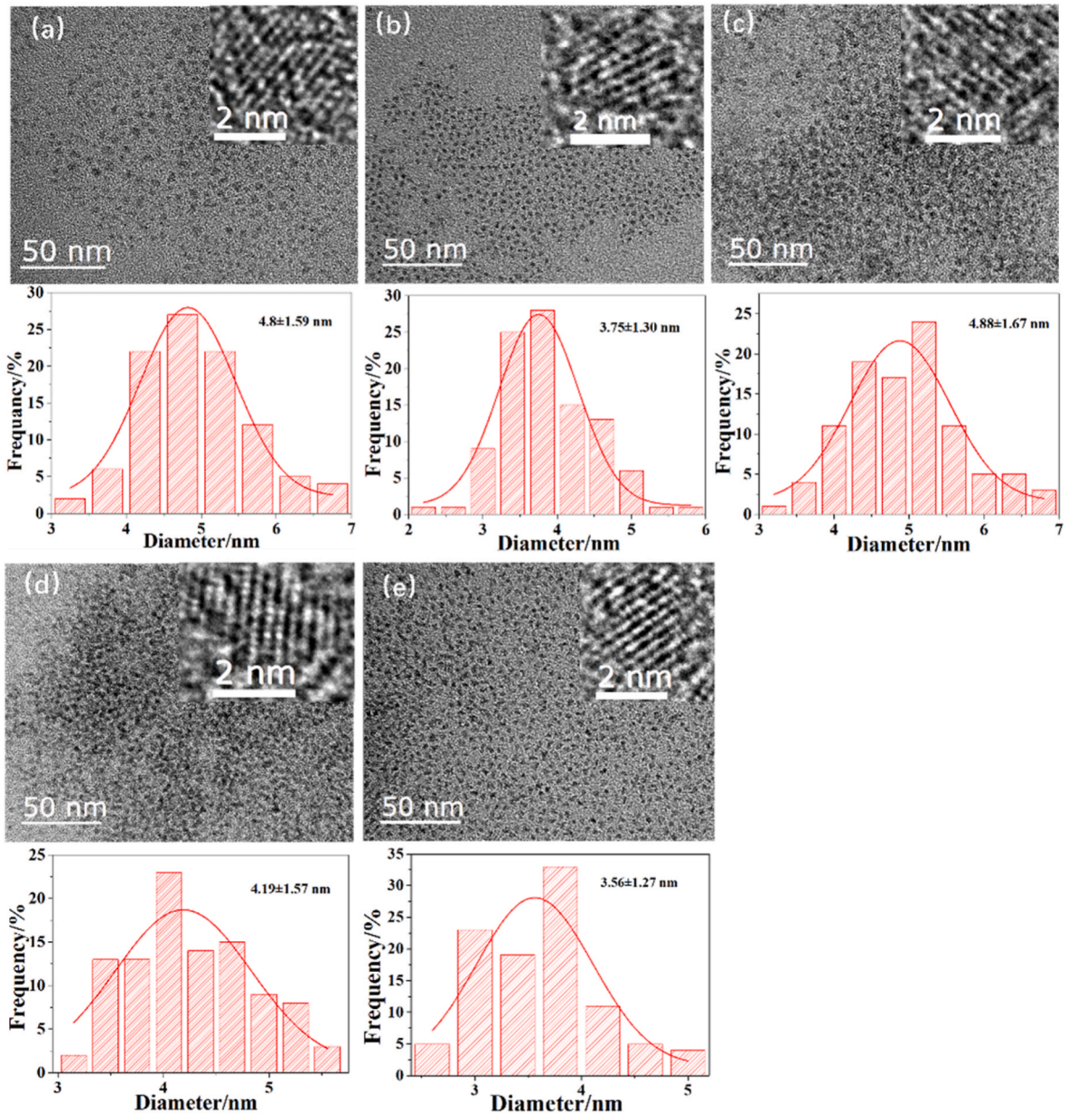

Fig. 3. TEM images (above) and correspond size distribution histograms (below) of InP/GaP/ZnS, InP–HF/GaP/ZnS, InP–HCl/GaP/ZnS, InP–HBr/GaP/ZnS, InP–HI/GaP/ZnS. (Insets at the top right of TEM images are the correspond HR-TEM images).

The inset pictures of Fig. 2(a–e) showed the photographs of InP, InP-HA, InP-HA/GaP and InP-HA/GaP/ZnS taken under 365 nm illumination. QDs became brighter along with the halogen acid treatment and shell coating expect the QDs treated with HI. During the synthesis process of QDs, the solution brightened significantly after addition of HF, HCl and HBr, while the solution became turbid after addition of HI. The PL QY of InP core increased from 13% to 67%, from 8% to 53%, from 15% to 27% after HF, HCl, HBr treatment respectively, while the PL QY of InP core decreased from 23% to 5% after HI treatment. Halogen acids used in the experiments all contain water. A small amount of water can improve the optical performance of QDs [32,33]. During the synthesis process of QDs with HI treatment, liquid droplets continuously return to the flask, resulting in the partial quenching of QDs. The water evaporated rapidly when HF, HCl and HBr were injected, and the backflow of liquid droplets was not obvious. The PL QY of InP/GaP/ZnS treated with HF, HCl, HBr and HI were 96%, 81%, 72% and 51%, while the PL QY of InP/GaP/ZnS without halogen acid treatment was 73%. That is to say, HF and HCl are beneficial to improve the optical properties of QDs, HBr especially HI are not conductive to promote the PL QY of QDs. It is widely known that F^- and Cl^- are hard bases, Br^- is the junction base and I^- is the soft base, In^{3+} is hard acid. According to the hard-soft acid-base (HSAB) theory, In^{3+} can form a strongest bond with F^- and Cl^-, followed by Br^-, the coordination effect of In^{3+} and I^- is the weakest. The HF and HCl can etch the oxidative layer, the F^- and Cl^- can also passivate the surface indium dangling bonds in the form of atomic ligands.

In order to verify the effect of halogen acid, a series of tests and characterizations were carried out. Fig. 4(a) shows the XRD patterns of InP, InP-HA, InP-HA/GaP/ZnS QDs. The InP/GaP/ZnS QDs with and without HA treatment exhibit the similar XRD results. The reflection peak from the XRD pattern of InP core are not obvious and the FWHM of (111) plane is wide. The (220) plane of zinc blende structure of InP core start to appear after HA treatment. The InP-HA/GaP/ZnS QDs all have great crystallinity, all peaks that are indexed to the (111), (220), and

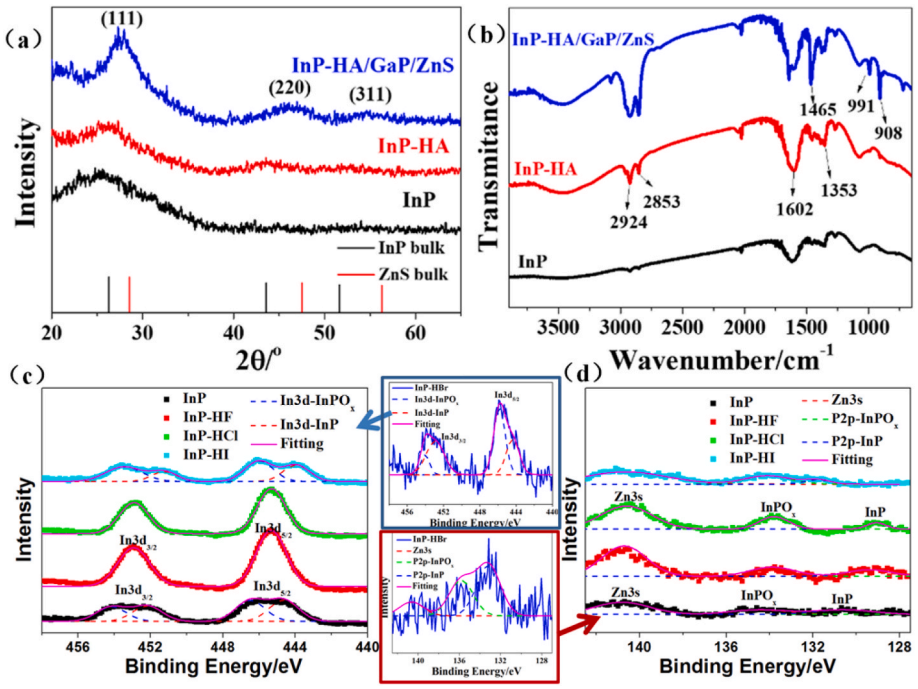

Fig. 4. (a) XRD patterns of InP, InP-HA, InP-HA/GaP/ZnS. Black and red lines indicate the peak positions of standard references of bulk zinc blende InP and ZnS, respectively (b) FTIR spectra of InP, InP-HA, InP-HA/GaP/ZnS QDs, (c) In 3d and (d) P 2p XPS spectra of InP and InP-HA.

(311) planes of zinc blende structure shift towards to ZnS peaks after coating the GaP and ZnS shells.

The FTIR spectra of InP, InP-HA, InP-HA/GaP/ZnS QDs presented in Fig. 4(b). The band at 3000-2840 cm^{-1} and 1470-1430 cm^{-1} are assigned to stretching vibration and bending of C–H group from Lauric acid, respectively [34]. The band 1550-1610 cm^{-1} and 1450-1400 cm^{-1} are assigned to the antisymmetric stretching vibration and symmetric stretching vibration of -COO^- from Lauric acid. The broad absorption of 940–1120 cm^{-1} is characteristic of the phosphate group [35]. However, the vibration of In–P and halogen bond were not found in the FTIR.

To further verify the effect of halogen acid, XPS characterization was also carried out. Fig. 4(c–d) present the In3d and P2p XPS spectra of InP and InP-HA. The In3d of InP contains two wide peaks located at 443–447 eV and 451–455 eV, and each peak can be fitted into two components which can be associated to $InPO_x$ and InP [36]. After HF and HCl treatment, the In_{3d} spectrum exhibits two narrow peaks which located at 444–447 eV ($3d_{5/2}$) and 452–454 eV ($3d_{3/2}$), which can be assigned to the InP. This indicated that the oxidative layer can be etched through HF and HCl. The XPS spectra of InP–HBr is placed separately in the middle of Fig. 4(c) and (d) because of the weak signal. Two peaks can be seen in the In_{3d} spectra, which can be assigned to the $InPO_x$ and InP through the decomposition of the peak. The In3d XPS spectra of InP–HI is very similar to that of InP, which indicate that HI has little effect to etch the oxidative layer of InP core. Fig. 4(d) shows the P2p XPS spectra of InP and InP-HA, the peak recorded at 139–141 eV is related to Zn3s because of introduction Zn precursor in the process of QDs synthesis [24]. For P2p XPS spectra of InP, the peak located at 132–136 eV is referred to $InPO_x$ [20,37], which is an indicative of phosphorus in an oxidized environment. The small peak recorded at 129–132 eV is related to InP, which is not obvious. This indicated that the InP core has been mostly oxidized. After HF and HCl treatment, the peak of binding energy in the range of 127–130 eV which is characteristic of the P^{3-} for InP become obvious, that is because the oxidative layer can be partially etched through HF and HCl. After HA treatment, the peak of $InPO_x$ decreased and the peak of InP increased relatively which indicated that the oxidative layer has been partially etched. The two peaks referred to InP and $InPO_x$ can also be seen in P2p spectra of InP–HBr. The P2p XPS spectra of InP–HI is very similar to that of InP, which also indicate that HI has little effect to etch the oxidative layer of InP core. Consequently, HF and HCl can etch the oxidative layer effectively, the effect of HBr is limited and HI is the weakest. The results are compounded with the previous HSAB theory.

From Fig. 5, the XPS survey spectrum of InP/GaP/ZnS QDs with and without halogen acid had the same result, which showed the presence of Zn2p, O1s, In3d and S2p with characteristic peaks at 1023, 532, 445 and 162 eV, respectively. The XPS test was carried out by coating QDs on glass substrate whose main component is SiO_2, so Si2p and O1s peaks were existed because of the thin coated film. The effect of the halogen acid can be reflected from the survey spectrum and high-resolution XPS of InP core and InP-HA core. From Fig. 5(b–e), the black lines showed the measured results of InP-HA cores, the red and blue lines were the corresponding fitting results. The F1s, Cl2p, Br3d and I3d were presented at high-resolution XPS pattern of InP–HF, InP–HBr, InP–HCl and InP–HI core, respectively. F1s with a characteristic peak located at about 686 eV [28]. The high-resolution XPS pattern of Cl2p, Br3d and I3d can fitted with two peaks. The signal of Br3d is weakest because of the thinnest film with strongest silicon peak in the survey spectrum, but the Br3d with characteristic peaks at about 68.1 and 68.7 eV could still be observed at high-resolution XPS pattern. Therefore, halogen can be adsorbed on the surface of InP core as surface ligand [38].

To obtain deep insight into HA effect to the PL emission mechanism of InP QDs, the time resolved photoluminescence has been applied to investigate its dynamic decay process. Fig. 6(a–e) show the transient PL spectra of InP QDs with and without HA treatment. The PL decay curves can be fitted using a triple-exponential function [39,40]:

$$I(t) = \sum_{i=1}^{3} B_i \, exp[-t / \tau_i]$$

Where the parameters τ_i are the decay time constants. B_i represent the amplitudes of each component. The percentage of each photoluminescence component can be calculated by follows [41]:

$$B_i\% = B_i\tau_i / (B_1\tau_1 + B_2\tau_2 + B_3\tau_3) \quad (i = 1, 2, 3)$$

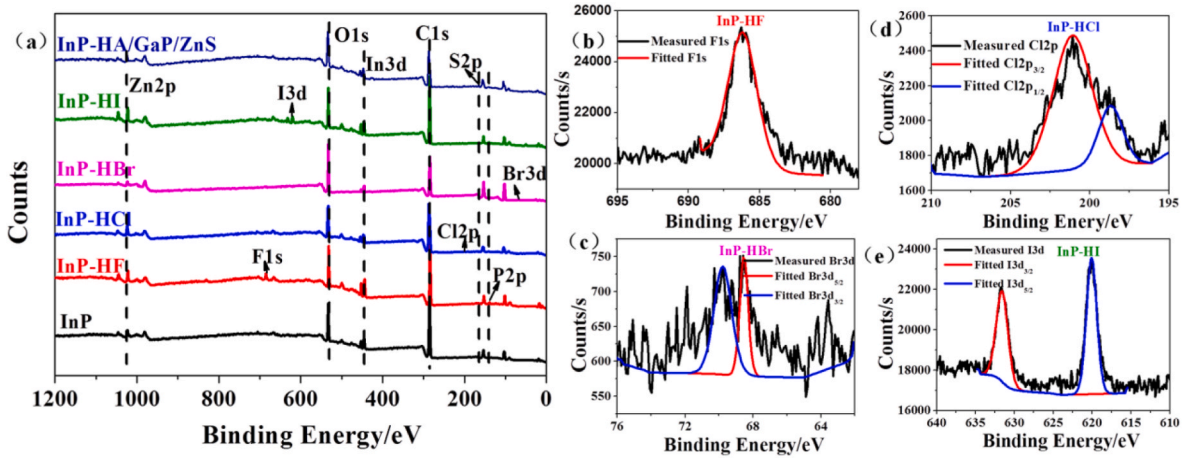

Fig. 5. (a) XPS spectra of InP, InP-HA, and InP-HA/GaP/ZnS. High-resolution XPS patterns of (b) F1s for InP–HF core, (c) Br3d for InP–HBr core, (d) Cl2p for InP–HCl core, and (e) I3d for InP–HI core.

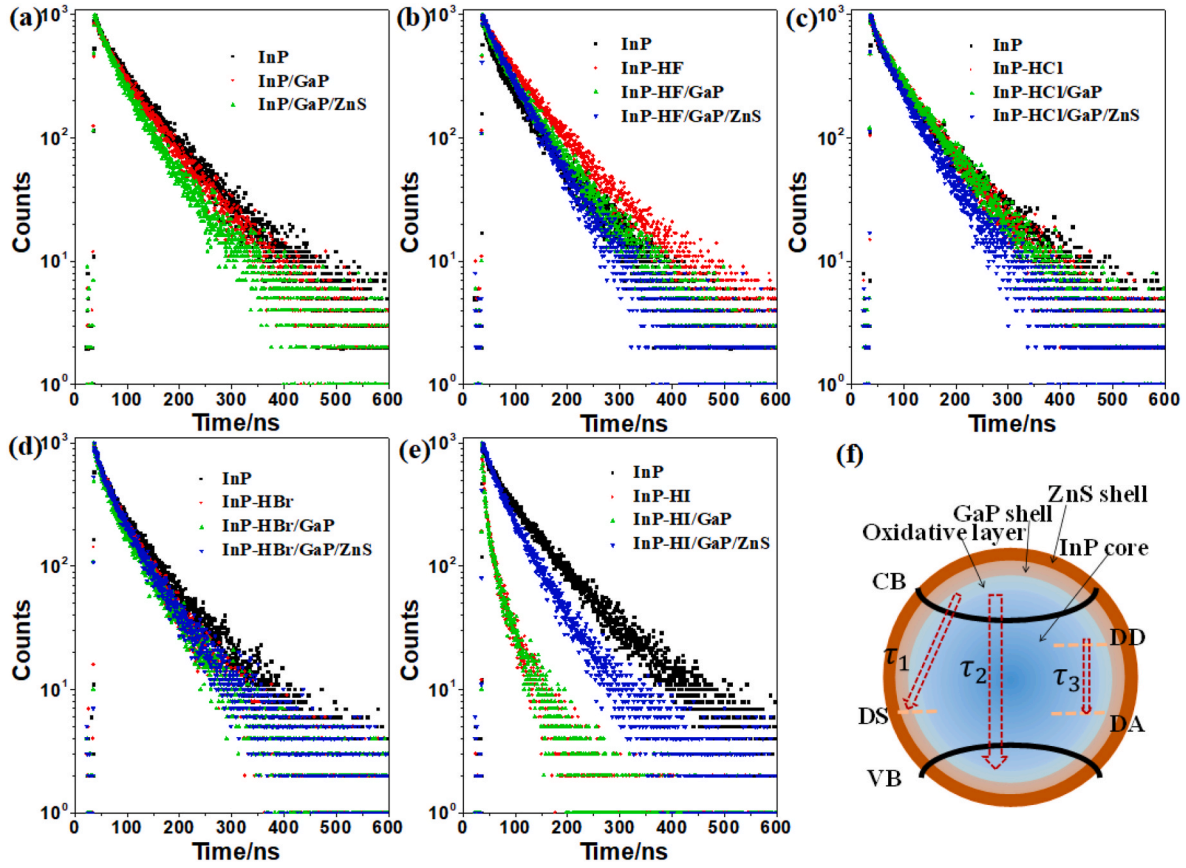

Fig. 6. (a) The transient PL spectra of InP, InP/GaP and InP/GaP/ZnS. The transient PL spectra of InP, InP-HA, InP-HA/GaP, InP-HA/GaP/ZnS with (b) HF, (c) HCl, (d) HBr, (e) HI etched, and (f) Schematic diagrams of recombination pathways observed in InP-HA/GaP/ZnS QDs.

The fitted results were summarized in Table 1. According to the results for transient PL spectra of InP/GaP/ZnS treated with HA, a model has been proposed to explain the charge carrier recombination processes as shown in Fig. 6(f). There are three major pathways for the charge carrier to recombine. The shorter lifetimes τ_1 could be assigned to the defects of surface (DS) related recombination. The longer lifetimes τ_2 could be referred to the radiative recombination of charge carriers through conduction band (CB) to valence band (VB). τ_3 could be assigned to recombination from intrinsic donor states (DD) to intrinsic acceptor states (DA) formed by the deep defect states such as vacancies, interstitials and antistites. In order to further explain the recombination pathways, schematic diagrams of recombination pathways observed in InP-HA/GaP/ZnS QDs has been shown in Fig. 6(f). Due to the intrinsic weak bonding nature and steric hindrance of organic ligands, the QDs have inherent multiple dangling bonds (DBs) on the surface atoms, such as In_{DB} and P_{DB} [42]. In and P are easy to oxidize to form oxidation defects, oxygen can occupy the indium and phosphorus sites to form O_{In} and O_P antistites [43]. Based on the irregularity of local crystal structure in semiconductor lattice, there are some defects, such as indium and phosphorus vacancies (V_{In} and V_P), interstitials (In_i and P_i) and antisites

Table 1
Summary parameters in term of transient PL spectra for InP-based QDs in the epitaxial processes.

	Sample	B_1 (B_1%)	τ_1 (ns)	B_2 (B_2%)	τ_2 (ns)	B_3 (B_3%)	τ_3 (ns)	PLQY (%)
InP/GaP/ZnS	InP	0.18 (2.55%)	8.26	0.31 (22.58%)	42.53	0.49 (74.87%)	89.2	21
	InP/GaP	0.15 (1.53%)	5.46	0.33 (21.13%)	34.29	0.51 (77.34%)	81.2	29
	InP/GaP/ZnS	0.05 (0.82%)	7.71	0.53 (33.52%)	29.59	0.42 (65.66%)	73.15	73
InP–HF/GaP/ZnS	InP	0.16 (0.75%)	2.04	0.36 (15.65%)	18.86	0.48 (83.60%)	75.55	13
	InP–HF	0.08 (0.25%)	2.00	0.28 (14.40%)	32.87	0.63 (85.35%)	86.57	67
	InP–HF/GaP	0.12 (2.19%)	9.33	0.46 (41.37%)	45.96	0.34 (56.44%)	84.82	65
	InP–HF/GaP/ZnS	0.10 (2.00%)	10.12	0.87 (90.76%)	52.72	0.02 (7.23%)	182.75	96
InP–HCl/GaP/ZnS	InP	0.29 (3.41%)	5.89	0.42 (34.27%)	40.83	0.31 (62.32%)	100.6	8
	InP–HCl	0.15 (0.95%)	3.3	0.37 (23.45%)	32.96	0.47 (75.60%)	83.63	53
	InP–HCl/GaP	0.15 (2.49%)	8.9	0.3 (18.77%)	33.49	0.52 (78.74%)	81.05	68
	InP–HCl/GaP/ZnS	0.16 (2.18%)	5.92	0.66 (64.38%)	42.39	0.16 (33.44%)	90.81	81
InP–HBr/GaP/ZnS	InP	0.3 (5.32%)	8.16	0.44 (43.94%)	45.98	0.23 (50.74%)	101.59	15
	InP–HBr	0.16 (1.84%)	4.66	0.34 (18.73%)	22.37	0.48 (79.43%)	67.21	27
	InP–HBr/GaP	0.18 (2.07%)	4.23	0.41 (26.13%)	23.43	0.38 (71.80%)	69.46	23
	InP–HBr/GaP/ZnS	0.2 (4.11%)	8.36	0.56 (55.44%)	40.29	0.18 (40.45%)	91.44	72
InP–HI/GaP/ZnS	InP	0.19 (1.30%)	3.98	0.35 (20.55%)	34.02	0.47 (78.15%)	96.37	23
	InP–HI	0.41 (5.89%)	1.42	0.44 (34.28%)	7.7	0.16 (59.83%)	36.95	5
	InP–HI/GaP	0.53 (9.97%)	1.87	0.37 (35.59%)	9.56	0.13 (54.44%)	41.62	4
	InP–HI/GaP/ZnS	0.34 (15.99%)	20.98	0.61 (75.20%)	55	0.02 (8.81%)	196.58	51

(In_P and P_{In}) [44]. In addition, due to the Zn precursor was added at the beginning of the synthesis of InP core, the zinc can occupy the indium site to from Zn_{In} antistite [45]. It should be pointed out that a number of different charge states could be exsited, take indium vacancies for example, there may be exsit V_{In}^{2+}, V_{In}^{+}, V_{In}^{0}, V_{In}^{-}, V_{In}^{2-}, and V_{In}^{3-} [46].

For InP/GaP/ZnS without HA treatment, the B_1% and B_3% decreased, while B_2% and PL QY increased after coating with GaP and ZnS shells, which indicate that the some defects especailly surface defects like P_{DB} and In_{DB} have been partly passivated upon shells growth. However, the B_3% value is 65.66% which is still very large, that is because the deep defects such as P_{In}, In_P, P_i, Zn_{In} have still existed. For InP–HF/GaP/ZnS, the B_1%, B_3% value decreased, while B_2% and PL QY increased after HF treatment and shell coating, which indicated that the surface oxidative defect states such as O_{In} and O_P have been reduced by HF etching, and also the dangling bonds such as P_{DB} and In_{DB} have been passivated by F^- in the form of atomic ligands. Moreover, the radiative recombination of charge carriers through conduction band to valence band increased. The large B_2% value which is 90.76% indicated that the InP–HF/GaP/ZnS almost belong to single channel radiative recombination, which made the PL QY up to 96%. The transient PL of InP/GaP/ZnS treated with HCl and HBr is similar to that of QDs treated with HF. For InP–HI/GaP/ZnS, the B_1% value of InP core increased after HI treatment, which indicated that a lot of surface defects still existed in InP core. The PL QY of InP–HI is only 5%, that is because the oxidative defects on the surface of the InP core has not been removed by HI and the adding of HI has brought other defects. The B_2% value increased to some extent after coating with ZnS shell, the final PL QY of InP–HI/GaP/ZnS is 51%.

In summary, for InP core without HA treatment, there are lot of surface defects and deep defects caused by surficial oxidative layer and irregular crystal structure, which resulted in the low PL QY of InP cores. After treated with HF, HCl and HBr, the contribution of τ_1 decreased, while the recombination of the recombination of electron-hole pairs on the CB and VB increased, which made the PL QY improvement. That is because the oxidative defects on the InP core has been partly removed by HF, HCl and HBr treatment and the dangling bonds has also been passivated by F^-, Cl^- and Br^-, which can reduce the amount of surface defects on the InP core. The defects have been passived further after coating with GaP and ZnS shells, and the contribution of τ_2 increased. Hence, the InP-HA/GaP/ZnS QDs exhibit the remarkable PL QY, especially the PL QY of InP–HF/GaP/ZnS QDs can reach to 96%.

4. Conclusion

In the present work, the InP/GaP/ZnS QDs with HF, HCl, HBr and HI have been synthesized respectively by halogen acid in-situ injection method, and the effect of luminescence properties of InP/GaP/ZnS QDs with halogen acid treatment have been studied. The results show that HF and HCl are beneficial to improve the optical properties of QDs, HBr especially HI are not conductive to promote the PL QY of QDs, which are compounded with the HSAB theory. The InP QDs with HF treatment has the best luminescence properties with high PL QY of 96%. The XPS results showed that HF and HCl can etch the oxidative layer effectively, the F^- and Cl^- can also passivate the surface indium dangling bonds in the form of atomic ligands. The effect of HA treatment on the electron-hole pairs recombination dynamics of InP-HA/GaP/ZnS has been investigated using transient PL spectra. The possible defects existed in the InP QDs has been summarized and a model of various charge carrier recombination process has been proposed. After HA treatment, the PL QY improved significantly which can be attributed to the recombination of electron-hole pairs through radiative pathways mainly from the CB and VB. The InP/GaP/ZnS QDs treated with HF and HCl has good optical properties, which can offer great potential for advanced optoelectronic devices.

Credit author statement

Yanqing Zhu: Investigation, Data curation, Formal analysis, Writing – original draft. **Cong Shen**: Investigation, Data curation, Software, Writing – review & editing. **Xueqing Xu**: Funding acquisition, Project administration, Resources. **Jianhua Zou**: Supervision, Writing – review & editing. **Lei Wang**: Writing – review & editing. **Xudong Cheng**: Supervision, Visualization. **Jingqiu Liang**: Supervision, Writing – review & editing. **Xiudi Xiao**: Funding acquisition, Project administration, Resources. **Gang Xu**: Supervision, Writing – review & editing.

Declaration of competing interest

The authors declare that they have no known competing financial interests or personal relationships that could have appeared to influence the work reported in this paper.

Data availability

Data will be made available on request.

Acknowledgments

This work was supported by Science and Technology Planning Project of Guangzhou [No. 202007020004], Strategic Priority Research Program of the Chinese Academy of Sciences, China [No. XDA21061001].

Appendix A. Supplementary data

Supplementary data to this article can be found online at https://doi.org/10.1016/j.jlumin.2022.119651.

References

[1] Y. Shu, X. Lin, H. Qin, Z. Hu, Y. Jin, X. Peng, Quantum dots for display applications, Angew. Chem. 59 (2020) 22312–22323.
[2] H.B. Jalali, S. Sadeghi, I.B. Dogru Yuksel, A. Onal, S. Nizamoglu, Past, present and future of indium phosphide quantum dots, Nano Res. 15 (2022) 4468–4489.
[3] M. Yu, M.H. Saeed, S. Zhang, H. Wei, Y. Gao, C. Zou, L. Zhang, H. Yang, Luminescence enhancement, encapsulation, and patterning of quantum dots toward display applications, Adv. Funct. Mater. 32 (2021), 2109472.
[4] K. He, C. Shen, Y. Zhu, X. Chen, Z. Bi, T. Marimuthu, G. Xu, X. Xu, Stable luminescent CsPbI3 quantum dots passivated by (3-aminopropyl)triethoxysilane, Langmuir : ACS J. surfaces Colloid 36 (2020) 10210–10217.
[5] Z. Hu, S. Liu, H. Qin, J. Zhou, X. Peng, Oxygen stabilizes photoluminescence of CdSe/CdS core/shell quantum dots via deionization, J. Am. Chem. Soc. 142 (2020) 4254–4264.
[6] A.L. Efros, L.E. Brus, Nanocrystal quantum dots: from discovery to modern development, ACS Nano 15 (2021) 6192–6210.
[7] X.K. Liu, W. Xu, S. Bai, Y. Jin, J. Wang, R.H. Friend, F. Gao, Metal halide perovskites for light-emitting diodes, Nat. Mater. 20 (2021) 10–21.
[8] K. He, Y. Zhu, Z. Bi, X. Chen, X. Xiao, G. Xu, X. Xu, Highly luminescent CsPbI3 quantum dots and their fast anion exchange at oil/water interface, Chem. Phys. Lett. 741 (2020), 137096.
[9] T. Kim, K.H. Kim, S. Kim, S.M. Choi, H. Jang, H.K. Seo, H. Lee, D.Y. Chung, E. Jang, Efficient and stable blue quantum dot light-emitting diode, Nature 586 (2020) 385–389.
[10] H. Qi, S. Wang, X. Jiang, Y. Fang, A. Wang, H. Shen, Z. Du, Research progress and challenges of blue light-emitting diodes based on II–VI semiconductor quantum dots, J. Mater. Chem. C 8 (2020) 10160–10173.
[11] Z. Yang, Q. Wu, X. Zhou, F. Cao, X. Yang, J. Zhang, W. Li, A seed-mediated and double shell strategy to realize large-size ZnSe/ZnS/ZnS quantum dots for high color purity blue light-emitting diodes, Nanoscale 13 (2021) 4562–4568.
[12] J. Ning, U. Banin, Magic size InP and InAs clusters: synthesis, characterization and shell growth, Chem. Commun. 53 (2017) 2626–2629.
[13] Y.-H. Won, O. Cho, T. Kim, D.-Y. Chung, T. Kim, H. Chung, H. Jang, J. Lee, D. Kim, E. Jang, Highly efficient and stable InP/ZnSe/ZnS quantum dot light-emitting diodes, Nature 575 (2019) 634–638.
[14] Z. Wu, P. Liu, W. Zhang, K. Wang, X.W. Sun, Development of InP quantum dot-based light-emitting diodes, ACS Energy Lett. 5 (2020) 1095–1106.
[15] X. Jiang, Z. Fan, L. Luo, L. Wang, Advances and challenges in heavy-metal-free InP quantum dot light-emitting diodes, Micromachines 13 (2022).
[16] J.-Y. Yoo, S.A. Park, W.H. Jung, C.W. Lee, J.S. Kim, J.-G. Kim, B.D. Chin, Effect of dithiocarbamate chelate ligands on the optical properties of InP/ZnS quantum dots and their display devices, Mater. Chem. Phys. 253 (2020), 123415.
[17] S.-R. Son, K.-P. Yang, J. Park, J.H. Lee, K. Lee, Highly efficient and eco-friendly InP-based quantum dot light-emitting diodes with a synergetic combination of a liquid metal cathode and size-controlled ZnO nanoparticles, Mater. Chem. Phys. 287 (2022), 126322.
[18] J.L. Stein, W.M. Holden, A. Venkatesh, M.E. Mundy, A.J. Rossini, G.T. Seidler, B. M. Cossairt, Probing surface defects of InP quantum dots using phosphorus Kα and kβ X-ray emission spectroscopy, Chem. Mater. 30 (2018) 6377–6388.
[19] M.D. Tessier, E.A. Baquero, D. Dupont, V. Grigel, E. Bladt, S. Bals, Y. Coppel, Z. Hens, C. Nayral, F. Delpech, Interfacial oxidation and photoluminescence of InP-based core/shell quantum dots, Chem. Mater. 30 (2018) 6877–6883.
[20] Y.C. Pu, H.C. Fan, J.C. Chang, Y.H. Chen, S.W. Tseng, Effects of interfacial oxidative layer removal on charge carrier recombination dynamics in InP/ZnSexS1-x core/shell quantum dots, J. Phys. Chem. Lett. 12 (2021) 7194–7200.
[21] C. Shen, Y. Zhu, H. Tao, J. Li, J. Zou, L. Wang, J. Liang, X. Xiao, X. Xu, G. Xu, Blue-Emitting InP/GaP/ZnS quantum dots with enhanced stability by siloxane capping: implication for electroluminescent devices, ACS Appl. Nano Mater. 5 (2022) 2801–2811.
[22] Y. Kim, S. Ham, H. Jang, J.H. Min, H. Chung, J. Lee, D. Kim, E. Jang, Bright and uniform green light emitting InP/ZnSe/ZnS quantum dots for wide color gamut displays, ACS Appl. Nano Mater. 2 (2019) 1496–1504.
[23] H. Zhang, N. Hu, Z. Zeng, Q. Lin, F. Zhang, A. Tang, Y. Jia, L.S. Li, H. Shen, F. Teng, Z. Du, High-Efficiency green InP quantum dot-based electroluminescent device comprising thick-shell quantum dots, Adv. Opt. Mater. 7 (2019), 1801602.
[24] C. Shen, Y. Zhu, Z. Li, J. Li, H. Tao, J. Zou, X. Xu, G. Xu, Highly luminescent InP–In(Zn)P/ZnSe/ZnS core/shell/shell colloidal quantum dots with tunable emissions synthesized based on growth-doping, J. Mater. Chem. C 9 (2021) 9599–9609.
[25] W. Zhang, S. Ding, W. Zhuang, D. Wu, P. Liu, X. Qu, H. Liu, H. Yang, Z. Wu, K. Wang, X.W. Sun, InP/ZnS/ZnS core/shell blue quantum dots for efficient light-emitting diodes, Adv. Funct. Mater. 30 (2020), 2005303.
[26] W. Yang, Y. Yang, A.L. Kaledin, S. He, T. Jin, J.R. McBride, T. Lian, Surface passivation extends single and biexciton lifetimes of InP quantum dots, Chem. Sci. 11 (2020) 5779–5789.
[27] N.A.J. Mii O, I synthesis and characterization of binary and ternary III-V quantum dots, J. Lumin. 70 (1996) 95–107.
[28] T.-G. Kim, D. Zherebetskyy, Y. Bekenstein, M.H. Oh, L.-W. Wang, E. Jang, A. P. Alivisatos, Trap passivation in indium-based quantum dots through surface fluorination: mechanism and applications, ACS Nano 12 (2018) 11529–11540.
[29] A. Berg, K. Mergenthaler, M. Ek, M.-E. Pistol, L. Reine Wallenberg, M.T. Borgström, In situetching for control over axial and radial III-V nanowire growth rates using HBr, Nanotechnology 25 (2014), 505601.
[30] T.T.T. Vu, T. Zehender, M.A. Verheijen, S.R. Plissard, G.W.G. Immink, J.E. M. Haverkort, E.P.A.M. Bakkers, High optical quality single crystal phase wurtzite and zincblende InP nanowires, Nanotechnology 24 (2013), 115705.
[31] H. Zhang, X. Ma, Q. Lin, Z. Zeng, H. Wang, L.S. Li, H. Shen, Y. Jia, Z. Du, High-brightness blue InP quantum dot-based electroluminescent devices: the role of shell thickness, J. Phys. Chem. Lett. 11 (2020) 960–967.
[32] P. Ramasamy, B. Kim, M.S. Lee, J.S. Lee, Beneficial effects of water in the colloidal synthesis of InP/ZnS core-shell quantum dots for optoelectronic applications, Nanoscale 8 (2016) 17159–17168.
[33] A.N. Mnoyan, A.G. Kirakosyan, H. Kim, H.S. Jang, D.Y. Jeon, Electrostatic stabilized InP colloidal quantum dots with high photoluminescence efficiency, Langmuir : ACS J. surfaces Colloid 31 (2015) 7117–7121.
[34] W.E. Mahmoud, A.A. Al-Ghamdi, L.M. Bronstein, Structural, morphological and optical behavior of In1-xHfxP films synthesized via 2,3-di(tetradecanoyloxy)propyl tetradecanoate assisted sol–gel technique for infrared photodiode applications, Opt Laser. Technol. 134 (2021), 106625.
[35] H.Y. Fudong Wang, Jingbo Li, Qingling Hang, Dmitry Zemlyanov, C. Patrick, Gibbons, Lin-Wang Wang, David B. Janes, William E. Buhro, Spectroscopic properties of colloidal indium phosphide quantum wires, J. Am. Chem. Soc. 127 (2007) 18.
[36] P. Ramasamy, B. Kim, M.-S. Lee, J.-S. Lee, Beneficial effects of water in the colloidal synthesis of InP/ZnS core–shell quantum dots for optoelectronic applications, Nanoscale 8 (2016) 17159–17168.
[37] A. Singh, C. Sharma, M. Kumar, R. Kumari, R. Srivastava, S.N. Sharma, Enhanced luminescence efficiency of wet chemical route synthesized InP-based quantum dots by a novel method: probing the humidity sensing properties, J. Lumin. 198 (2018) 108–116.
[38] P. Liu, Y. Lou, S. Ding, W. Zhang, Z. Wu, H. Yang, B. Xu, K. Wang, X.W. Sun, Green InP/ZnSeS/ZnS core multi-shelled quantum dots synthesized with aminophosphine for effective display applications, Adv. Funct. Mater. 31 (2021), 2008453.
[39] O.V. Ovchinnikov, M.S. Smirnov, N.V. Korolev, P.A. Golovinski, A. G. Vitukhnovsky, The size dependence recombination luminescence of hydrophilic colloidal CdS quantum dots in gelatin, J. Lumin. 179 (2016) 413–419.
[40] M.S. Smirnov, O.V. Ovchinnikov, IR luminescence mechanism in colloidal Ag2S quantum dots, J. Lumin. 227 (2020), 117526.
[41] W. Shen, H. Tang, X. Yang, Z. Cao, T. Cheng, X. Wang, Z. Tan, J. You, Z. Deng, Synthesis of highly fluorescent InP/ZnS small-core/thick-shell tetrahedral-shaped quantum dots for blue light-emitting diodes, J. Mater. Chem. C 5 (2017) 8243–8249.
[42] E. Cho, T. Kim, S.-m. Choi, H. Jang, K. Min, E. Jang, Optical characteristics of the surface defects in InP colloidal quantum dots for highly efficient light-emitting applications, ACS Appl. Nano Mater. 1 (2018) 7106–7114.
[43] B.W.W. Masahide Inuishi, Deep level transient spectroscopy of interface and bulk trap states in InP metal oxide semiconductor structures, Thin Solid Films 103 (1983) 141–153.
[44] G. Hirt, D. Hofmann, F. Mosel, N. Schafer, G. Muller, Annealing and Bulk Crystal Growth of Undoped InP under Controlled P-Pressure: a Perspective for the Preparation of Undoped SI InP?, Indium Phosphide & Related Materials, Third International Conference. IEEE., 1991, pp. 16–19.
[45] M. Yamada, P.K. Tien, R.J. Martin, R.E. Nahory, A.A. Ballman, Double zinc diffusion fronts in InP—theory and experiment, Appl. Phys. Lett. 43 (1983) 594–596.
[46] A.P. Seitsonen, R. Virkkunen, M.J. Puska, R.M. Nieminen, Indium and phosphorus vacancies and antisites in InP, Phys. Rev. B 49 (1994) 5253–5262.